

Nitrogen-induced transformation of vitamin C into up-converting carbon nanodots with enhanced optical response for sensing and bioimaging in the visible-NIR range

*M. Carmen Ortega-Liebana^{a,b}, M. Mar Encabo-Berzosa^{a,b}, M. Jose Ruedas-Ramada^c,
Jose L. Hueso^{a,b,*}*

^aInstitute of Nanoscience of Aragon (INA) and Department of Chemical Engineering and Environmental Technology, University of Zaragoza, 50018 Zaragoza, Spain.

^bNetworking Research Center on Bioengineering, Biomaterials and Nanomedicine (CIBER-BBN), 28029 Madrid, Spain.

^cDepartment of Physical Chemistry, Faculty of Pharmacy, University of Granada, E-18701 Granada, Spain.

*Corresponding author: Email: jlhueso@unizar.es /Telephone: +34876555442

ABSTRACT

Water-soluble, biocompatible, and photo-luminescent carbon nanodots have been obtained from the rationalized carbonization of vitamin C, a well-known antioxidant molecule in the presence of an amine co-reactant. Herein, we describe the positive influence of N-doping to induce a unique pH-dependent lifetime decay response that would be potentially attractive in biological backgrounds with intrinsic fluorescence fluctuations. In addition, the selectivity and sensitivity of the N-containing carbon nanoprobe towards the detection of copper ions at ppm levels is critically enhanced in comparison with the un-doped counterpart, especially in the near-infrared (NIR) range. Finally, the up-converting properties have been also successfully applied to image tumor cells in the visible range and remarkably in the NIR region where minimal tissue and water absorption and maximum penetration depth is expected.

1. Introduction

Semiconducting quantum dots (QDs) and up-converting rare-earth based nanoparticles (UCNPs) represent two of the most widespread fluorescent systems successfully developed in recent years for sensing and imaging applications.[1, 2] Recently, a new sort of luminescent carbon-based structures including graphene dots, carbon nanotubes (CNTs) or carbogenic nanodots (hereafter CNDs) has emerged as a competitive alternative to overcome the major concerns arising from QDs and UCNPs:[3-13] (i) the inherent toxicity of certain components that burdens their biomedical applications; the threat to both at biological and environmental levels; (ii) the requirement of multiple and tedious steps during synthesis and purification; (iii) the requirement of high-boiling solvents and ligand exchange to make them water-soluble or optically active in the near-infrared (NIR) range. In this regard, CNDs exhibit appealing properties such as an inexpensive and abundant variety of potential precursors, high resistance to photo-bleaching, wide emission spectra in the whole UV-Vis-NIR range, good colloidal stability in water and minimal cytotoxicity. Remarkably, certain types of CNDs have also shown up-converting properties to convert longer wavelength radiation from the NIR range into shorter wavelength emitting in the visible range thereby expanding the potential application of these carbogenic dots in bioimaging, sensing, photocatalysis, solar cells and theranostics.[3, 14-29]

Different bottom-up and top-down synthesis approaches have been recently developed and reviewed elsewhere.[30-33] Among them, the hydrothermal carbonization of low-cost raw materials is considered as one of the most simple, straightforward and cost-effective methods to successfully obtain CNDs. Furthermore, the simultaneous or subsequent addition of co-reactants containing N, P or S groups has been identified as a

crucial step to provide CNDs with up-converting properties, even though the origin of such optical behavior is not fully understood yet.[5, 34] Nevertheless, there is still room to further explore and optimize the full potential of these nanomaterials and their applications. Herein, we report on the effect of adding ethanolamine (EN) as a co-reactant containing a short chain terminal amine group during the hydrothermal carbonization of vitamin C (ascorbic acid-AA). Interestingly, we have observed a different and sensitive optical response upon pH variations or as selective probe for copper ion detection in comparison with its un-doped counterpart. Furthermore, the presence of N species has also enabled an up-converting response successfully applied to the direct imaging of cells in the NIR window where minimal tissue damage and maximum penetration depth is expected.[35, 36]

2. Experimental Section

2.1. Chemicals

L-Ascorbic acid (AA), ethanolamine (EN), lead (II) nitrate ($\text{Pb}(\text{NO}_3)_2$), cadmium nitrate tetrahydrate ($\text{Cd}(\text{NO}_3)_2 \cdot 4\text{H}_2\text{O}$), iron (III) sulphate monohydrate ($\text{Fe}_2(\text{SO}_4)_3$), silver nitrate (AgNO_3), zinc sulfate heptahydrate ($\text{ZnSO}_4 \cdot 7\text{H}_2\text{O}$), mercury (II) chloride (HgCl_2) and copper (II) sulfate (CuSO_4) were obtained from Sigma-Aldrich. All chemicals were of analytical purity grade. 10 KDa molecular weight cut off (MWCO) membranes (Amicon Ultra-15, Millipore) were also obtained from Sigma-Aldrich.

2.2. Synthesis and purification of carbon dots

To synthesize the un-doped carbon nanodots, 1 M solution of L-ascorbic acid, as the carbon source, and 10 mL triple distilled water were mixed in a beaker with a magnetic blender, the solution was then transferred into a 25 mL Teflon-lined stainless-steel autoclave and was heated at a constant temperature of 250 °C for 4 hours. The resulting

solution was cooled at room temperature and was centrifuged at 6000 rpm for 10 min to remove agglomerated particles. The supernatant containing carbon nanomaterials was filtered through a 0.10 μm PTFE membrane (WhatmanTH) membrane to further remove large particles. The brownish yellow supernatant was then dialyzed against ultrapure water through a dialysis membrane for 5 h. An analogous procedure was carried out to synthesize the N-doped carbon nanodots but replacing the initial 1 M solution of L-ascorbic acid by a solution containing a 1:3 molar ratio (ethanolamine: ascorbic acid).

2.3. Characterization techniques

The morphologies and particle size distributions were determined by transmission electron microscopy (TEM) (FEI Tecnai T20 and F30, operated at 200-300 kV, respectively). To prepare the samples, the nanoparticle suspensions were diluted with water prior to casting on a holey carbon TEM grid. The functionalization of the CNDs surface was analyzed by Fourier transform infrared (FTIR) spectroscopy (Bruker Vertex 70 FTIR spectrometer) and X-ray photoelectron spectroscopy (XPS) with an Axis Ultra DLD (Kratos Tech.). A monochromatic Al K α source (1486.6 eV) was employed with multiple runs at 12 kV, 10 mA and pass energy of 20 eV was used. The binding energies were calibrated to the internal C1s (284.2 eV) standard. Analyses of the peaks were performed with CasaXPS software, using a weighted sum of Lorentzian and Gaussian component curves after Shirley background subtraction. Steady-state fluorescence emission spectra were collected on a JASCO FP-6500 spectrofluorometer equipped with a 450 W xenon lamp for excitation, with temperature controller ETC-273T at 25 °C, using 5 \times 10 mm cuvettes and a LS55 Fluorescence Spectrometer (PerkinElmer) equipped with a xenon arc lamp as the light source and a quartz cell (10 x 10 mm). The excitation wavelengths used in the experiments to record the emission

spectra were 400 and 740 nm. Both excitation and emission slits were 3 nm. Fluorescence decay traces of the different CNDs were recorded in the Time Correlated Single Photon Counting (TCSPC) mode using the FluoTime 200 fluorometer (PicoQuant, GmbH). Briefly, the samples were excited by a 405 nm Picosecond Pulsed Diode Laser (Edinburgh EPL405) with a 10 MHz repetition rate. The full width at half maximum of the laser pulse was ~ 90 ps. The fluorescence was collected after crossing through a polarizer set at the magic angle, and a 2 nm bandwidth monochromator. Fluorescence decay histograms were collected using a TimeHarp200 board, with a time increment per channel of 36 ps, at the emission wavelengths of 450, 460, and 470 nm. The histograms of the instrument response function (IRF) was determined using LUDOX scatterer, and sample decays were recorded until they typically reached 2×10^4 counts in the peak channel, since it is well known that complex decays can be well described by the simplest exponential models if the fitting is carried out from experimental data with a low number of CPC.

2.4. Quantum Yield calculations

The fluorescence quantum yields Φ of the different CNDs in aqueous solution were computed according to the equation 1[37] :

$$\Phi_S = \Phi_R \times F_S \times (1 - 10^{-A_R(\lambda_{ex})}) \times n_S^2 / F_R \times (1 - 10^{-A_S(\lambda_{ex})}) \times n_R^2 \quad (\text{eqn. 1})$$

The subscript S refers to the CND samples, R stands for the selected reference fluorophore (quinine sulfate, 0.1 M H₂SO₄) with known quantum yield (0.54), F stands for the corrected, integrated fluorescence spectra, $A(\lambda_{exc})$ denotes the absorbance at the used excitation wavelength λ_{exc} , and n represents the refractive index of the solvent. To minimize inner filter effects, the absorbance at the excitation wavelength λ_{exc} was kept under 0.1. The measurements were performed using 10 mm optical path length cuvettes

under right-angle (L-) arrangement and ‘magic angle’ conditions. The averages and standard uncertainties of Φ are computed from independent Φ measurements (2 conc. of sample \times 2 conc. of reference \times 2 excitation wavelengths λ_{exc}).

2.5. Time-resolved photoluminescence decays at different pH values

Time resolved photoluminescence decay traces were fitted using FluoFit 4.4 package (Picoquant GmbH). In all cases, PL decay traces were recorded at 450, 460 and 470 nm emission wavelengths, and the three decay traces were fitted globally with the decay times linked as shared parameters, whereas the pre-exponential factors were local adjustable parameters. The experimental decay traces were fitted to multi-exponential functions via a Levenberg-Marquard algorithm-based nonlinear least-squares error minimization deconvolution method. In all cases, three different exponential terms were used to fit the experimental decay traces. The quality of fittings was evaluated by the reduced chi-squared method, χ^2 , the weighted residuals and the correlation functions. In all cases, the best fits of the decay traces required a sum of three exponential decay functions to reach low χ^2 values as well as random distributions of the weighted residuals and auto-correlation function, indicators of the goodness of the fits (Figures S7 and S8 for CND and N-CND respectively). To compare the emission lifetime of the different CNDs at different concentrations and different pH media it was necessary to determinate their average lifetime using the equation 2[38]:

$$\tau_{ave} = \frac{\sum a_i \tau_i^2}{\sum a_i \tau_i} \quad (\text{eqn. 2})$$

where a_i are pre-exponential factors and τ_i the lifetimes obtained in the multi-exponential fitting of the decay curves of CNDs emission.

2.6. Quenching and interference experiments for detection of copper

The quenching by Cu^{2+} ions was initially described using the Stern-Volmer formalism (see eqn. 3), where I_0 represents the PL intensity of the N-CNDs in the absence of Cu^{2+} ; I corresponds the PL intensity observed in the presence of Cu^{2+} and K_{S-V} is the Stern-Volmer constant.

$$I_0/I = 1 + K_{S-V}[\text{Cu}^{2+}] \quad (\text{eqn. 3})$$

Although a linear dynamic response could be determined for copper (II) concentrations between 0.1-10 μM , the existence of a downward curvature suggests that all the surface of the CNDs are not equally accessible to the quenchers or an uneven functional group distribution. Therefore, a modified Stern-Volmer model (eqn. 4) was used to assess whether only a fraction of Cu^{2+} was being quenched [38, 39]

$$I_0/\Delta I = 1/(f_a K_a [\text{Cu}^{2+}]) + 1/f_a \quad (\text{eqn. 4})$$

where $\Delta I = (I_0 - I)$, f_a is the fraction of initial fluorescence that is accessible to the quencher and K_a is the Stern-Volmer quenching constant of the accessible fraction. For the quenching experiments, CNDs were incubated for 15 minutes with different targeted concentrations of ions ranging from 1×10^{-9} M to 1×10^{-4} M. Fe^{3+} , Hg^{2+} , Pb^{2+} , Cd^{2+} , Ag^+ and Zn^{2+} ions were checked individually in the same concentration ranges and as crossed-interferences in the presence of Cu^{2+} at equimolar concentrations of 1 and 10 μM . The samples were systematically excited at 400 nm and 740 nm.

2.7. Cell Viability Assays

The N-CNDs solutions used in the assay were obtained by diluting the stock solution in culture cell medium. The final concentration of water in the medium did not cause any osmotic imbalance. Human U251MG glioma cells were culture in Dulbecco's modifies Eagle's medium (DMEM, GIBCO) with 10% fetal bovine serum (FBS, GIBCO), 1%

penicillin/streptomycin and 1% amphotericin overnight. Then, cells were seeded into 96-well culture plate at a concentration of 7×10^3 cells per well in 100 μL of the above medium. After incubation at 37 °C in a 5% CO_2 -humidified incubator for 24 h, the medium was changed to 100 μL medium with C-dots (500 to 37,5 $\mu\text{g mL}^{-1}$ (serial dilutions)) and cells were cultured for another 24 h in contact with the different concentrations of N-CNDs. For studying the cytotoxicity we used Alamar-Blue assay (Invitrogen). This method is based on the reduction of resazurin to resorufin by mitochondrial oxidoreductases. After the N-CNDs incubation we removed the medium and washed with PBS. Then, cells were treated with 10% (v/v) of resazurin dye reagent prepared in DMEM medium. The plate was then placed in a 37°C/5% CO_2 incubator for 3h. After that the plate was read at 530 nm excitation and 590 nm emission wavelengths using a Synergy HT (Biotek) plate reader. Results are represented as percentage of the control (cells without N-CNDs treatments).

2.8. Cell cultures and Confocal Microscopy Bioimaging in the visible-NIR ranges

N-CNDs were diluted to 0.5 mg mL^{-1} concentrations for a stock solution. The N-CNDs solutions used in the assays (0.05 and 0.2 mg mL^{-1}) were obtained by diluting the stocks solution in culture cell medium. The final concentration of water in the medium did not cause any osmotic imbalance. Human U251MG glioma cells were cultured in Dulbecco's modified Eagle's medium (DMEM, GIBCO) with 10% fetal bovine serum (FBS, GIBCO), 1% penicillin/streptomycin and 1% amphotericin overnight. Cells were subsequently seeded on sterile cover-slips at a density of 50000 cells per well and were incubated during 24 h with the N-CNDs (0.05 and 0.2 mg mL^{-1}). Subsequently, cells were washed twice with PBS and fixed with 4% paraformaldehyde. The cover-slips were mounted and the samples were observed in an Olympus FV10-i OilType confocal

microscopy with a laser excitation source at 488 nm and analysed with the microscopy software. Analogous settings were utilized for both the control experiments (without N-CNDs) and the samples. Likewise, the experiments for the NIR imaging were carried out with the aid of a Leica SP5 HyD multi-photon microscope combining the flexibility of confocal imaging with the deep tissue imaging capability of multiphoton (or two-photon) microscopy. The titanium-sapphire infrared laser was tuned and optimized at 740 nm.

3. Results and Discussion

3.1. Synthesis and morpho-chemical characterization of the CNDs

The hydrothermal synthesis of the CNDs is summarized in Figure 1 and further detailed in the Experimental Section. A first synthesis of CNDs was carried out in the absence of the amine precursor (hereafter labelled as CND, see Figure 1) to clearly establish the influence of adding N species during the carbonization of AA (hereafter denoted as N-CNDs, Figure 1). Typically, an aqueous solution containing 10 mL of a 1 M solution of the organic precursor (AA or EN:AA 1:3 molar ratio) was mixed and magnetically stirred in a beaker for 10 minutes and then transferred into a Teflon-lined stainless-steel autoclave that was heated at 250 °C for 4 hours. Figures 2a-2b shows the morphologies and particle size distributions obtained by transmission electron microscopy (TEM) after purification (see Experimental Section). The CNDs retrieved from the hydrothermal carbonization of AA exhibited a quite homogeneous size distribution of 5.6 ± 1.1 nm (see Figure S1, Supporting Information) whereas the N-CNDs rendered smaller mean diameters of 3.3 ± 1.7 nm (see Figure S2, SI).

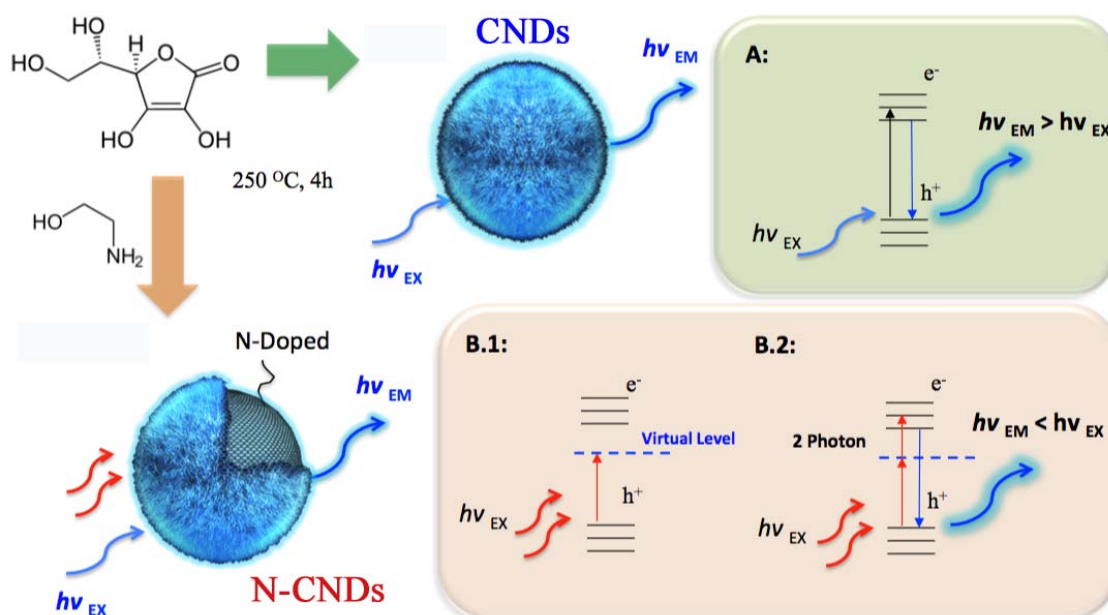


Figure 1. Hydrothermal carbonization of ascorbic acid at 250 °C in the absence and the presence of ethanolamine to obtain un-doped (CNDs) and N-modified carbon nanodots (N-CNDs); The colored charts (right) display the down-conversion and up-conversion mechanisms for each type of luminescent carbon dot.

The evaluation of the surface chemistry carried out by XPS showed an enrichment of nitrogen-containing groups in the N-CNDs with two main contributions centered at ca. 399 and 401 eV, respectively (Figure 2d). The former contributions have been previously assigned to N species present in terminal and bridge positions of carbon networks (-C-N-H/-C-N-C).[40] Likewise, the latter contribution is attributable to pyrrol-type rings (N₅) or alternatively to the presence of protonated primary amines (-NH₃⁺).[41] The O1s region revealed an increment of the fraction of oxygen species bonded to carbon species with sp³ configuration (typically aliphatic) at ca. 531 eV.[40] Finally, the evaluation of the C1s regions (Figures S3-S4, SI) and additional FT-IR spectroscopic analyses (Figure S5, SI) confirmed the presence of multiple C=O, C-O and C-OH surface groups. Interestingly, the absence of amide bond signatures also corroborated that N is predominantly present in the N-CNDs as dopant or as terminal amine group. The role of amine precursors with shorter alkyl chains as N-doping inducer has been also claimed in previous works.[42]

region and quantum yields (QYs) of 12% using quinine sulphate as reference (see Experimental Section). Remarkably, the N-CNDs exhibited up-conversion capabilities after the excitation in the NIR range (Figure 3b) and slightly higher QY values of 15%. Although the underlying mechanism has not been fully understood yet, it has been claimed that N atoms can provide additional energy levels to accommodate intermediate electronic transitions upon excitation with longer wavelength photons and favor the absorption of a second photon prior to the radiative recombination decay and facilitate the final emission of a single photon at shorter wavelengths (Figure 2b and Figure 1, Chart B).

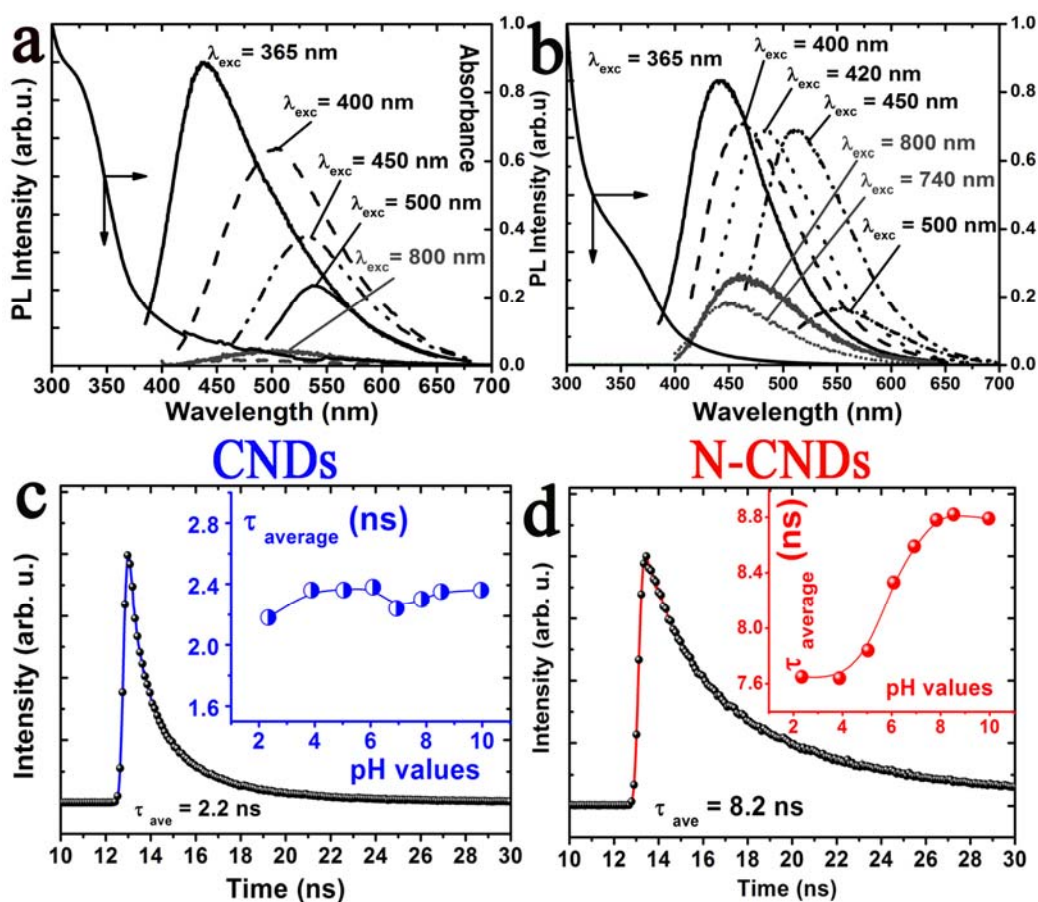


Figure 3. a) UV-Vis absorbance spectrum and wavelength-dependent photoluminescence emission spectra of the un-doped CNDs; b) UV-Vis absorbance and wavelength-dependent photoluminescence emission spectra of the N- CNDs displaying both down and up-conversion; c) Time-resolved fluorescence-decay curve of the un-doped CNDs exciting at 470 nm (inset: evolution of the average lifetimes at different pH values); d) Time-resolved fluorescence-decay curve of the N-CNDs exciting at 470 nm (inset: pH-dependent evolution of the average lifetime).

Another important effect of the addition of ethanolamine as co-reactant was observed in the variation of the time-resolved PL emission decays (Figures 3c-3d). These PL decays are correlated with the radiative and non-radiative pathways that an exciton undergoes to achieve electron-hole recombination and can be modified by changes on the surface environment.[1, 43]

The N-CNDs exhibited longer average PL lifetimes of 8.23 ± 0.06 ns in comparison with the PL lifetime averages of 2.24 ± 0.01 ns of the un-doped nanoparticles. A sum of three-exponential functions was required to adjust the PL decay traces (see also Experimental Section). The shortest fitting components have been previously attributed to intrinsic recombination of populated core states whilst the longer (slower) fitting components have been usually attributed to surface defects that give rise to trap and surface states. The major contribution of these latter components in the N-CNDs account for the induced variation at their surface composition as also suggested from XPS analysis (Figure 2). After the exponential fitting analyses of the PL decays, the intensity-weighted average lifetime (τ_{ave}) were calculated at different pH values (see Tables S1-S2). Interestingly, the calculated τ_{ave} of the N-CNDs showed a dependency on the pH value of the media, decreasing from 8.8 ns at alkaline conditions (pH > 8) to 7.6 ns when the pH was set below 4.5 (see inset in Figure 3d).

A linear response was identified in the pH range 4.5-8.0 where a great potential application for pH determination in biological samples such as endosomes (pH = 5-6.5) or some tumour cells (pH = 6.4-6.9) can be envisioned.[1, 43] Although this linear range is similar to other pH-related nanosensors,[1] the measurements based on average lifetimes offer several advantages in comparison with fluorescent-based analyses,

especially in terms of the acquisition of a reliable and unique signal regardless of the CNDs local concentration changes and the fluctuations associated to the intrinsic background fluorescence typically observed in biological samples. This fact minimizes the requirement of ratiometric nanoprobe[24] or multi-channel/multi-colour detection systems[43] and provides the N-CNDs with a remarkable potential for pH sensing applications.[24]

3.3. Sensing and bioimaging applications of the CNDs

3.3.1. Selective detection of copper ions in the visible-NIR range

The carbon dots were also systematically investigated as potential nanoprobe for the detection of ions and the presence of the amine co-reactant rendered an enhanced selective response towards the presence of copper ions (Figures 4a-4b) in comparison with the un-doped CNDs. The N-CNDs showed a selective quenching efficiency in the presence of Cu^{2+} while the other selected ionic species did not cause any significant change in the fluorescence intensity of the N-CNDs for the evaluated concentrations (up to 10^{-4} M) (Figure 4c). Only the presence of Fe^{3+} ions caused certain optical changes or interference at concentration levels higher than 3×10^{-5} M when using an excitation wavelength of 400 nm (Figures 4e-4f). This influence has been previously attributed to inner filter effects[44] caused by its strong absorption in that wavelength range and in the case of our up-converting N-CNDs could be minimized after selecting an excitation wavelength of 740 nm (Figure 4f)[3]. The quenching mechanism was described by the Stern-Volmer formalism and a modified approximation accounting for a fractional accessibility of the quenchers[39] (Figure 4d and Experimental Section).

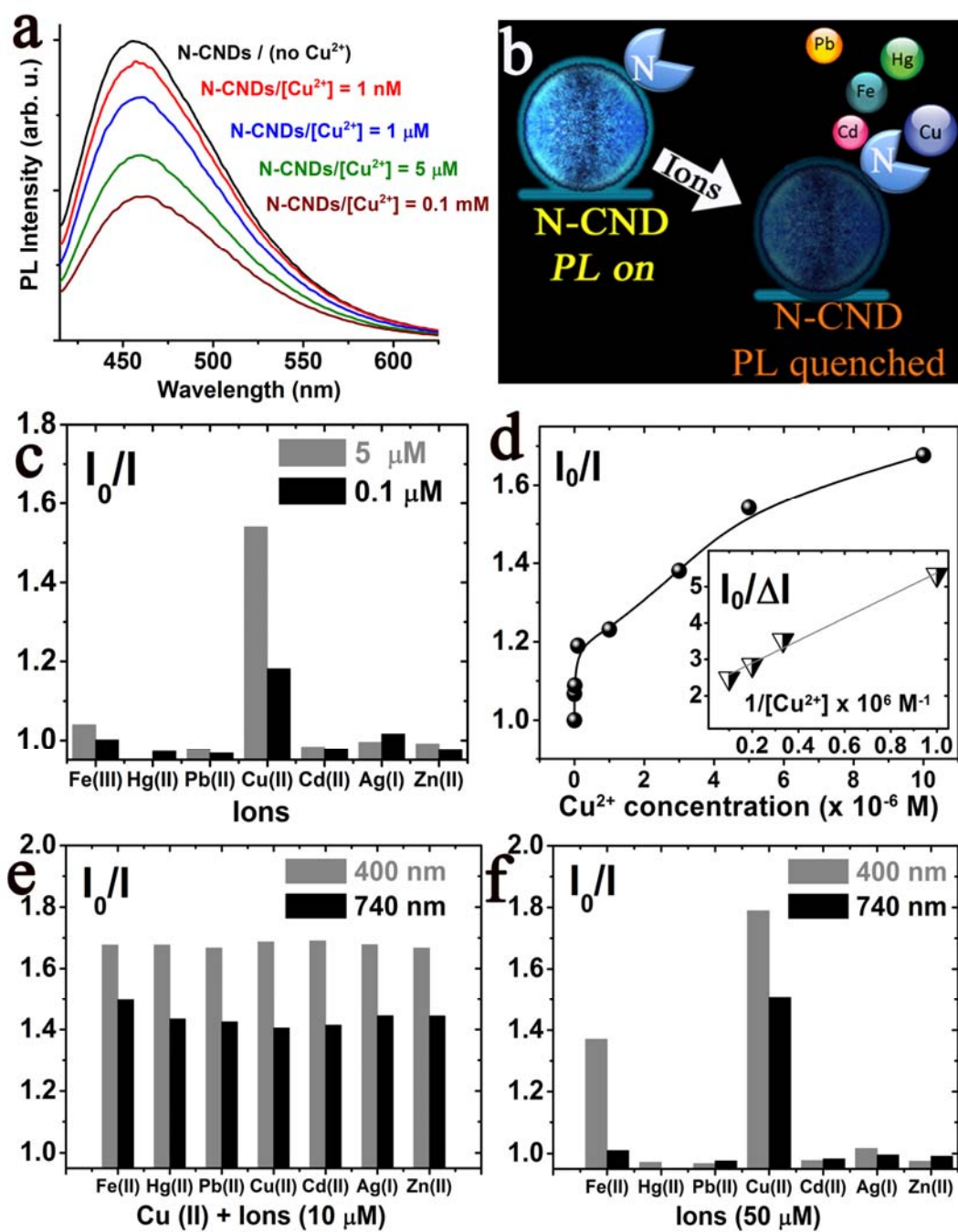


Figure 4. a) Photoluminescence spectra of N-CNDs in the presence of different concentrations of Cu^{2+} ($\lambda_{\text{exc}} = 400 \text{ nm}$); b) Scheme of the PL quenching effect induced by the presence of copper ions; c) Selectivity of the N-CNDs for Cu^{2+} in comparison with other tested ionic species ($\lambda_{\text{exc}} = 400 \text{ nm}$); d) Collisional quenching of the PL intensity of the CNDs by Cu^{2+} using the Stern-Volmer formalism and its modified approximation considering a fractional accessibility of quenchers (inset); e) PL response of the N-CNDs in the presence of Cu^{2+} and a second interference ion (equimolar concentrations of $10 \text{ }\mu\text{M}$). Excitation wavelengths selected at 400 nm and 740 nm respectively; f) Evaluation of the preferential interference of Fe-II ions at concentrations higher than $30 \text{ }\mu\text{M}$ and how the inner filter effect can be dramatically diminished upon excitation at 740 nm , taking advantage of the up-converting capabilities of the N-CNDs.

A linear response range towards the Cu^{2+} detection was determined between 0.1 – 10 μM (Figure 4d) with a limit of detection of 0.1 μM and a 44% of accessible fraction to quenchers (see Experimental Section). This response as selective nanoprobe for copper ions fits within the range of previously reported fluorescent nanoparticles[3, 18, 44-46] and meets the detection limit criteria established by the Environmental Protection Agency (EPA) as a priority pollutant.[2, 3, 45, 46]

3.3.2. Evaluation as biocompatible cell biomarkers in the visible-NIR range

Finally, taking into account the greater biocompatibility of carbon nanodots in comparison with other nanostructured semiconductors containing heavy metals, the N-CNDs were also successfully evaluated as fluorescent biomarkers of U251MG glioma cells both under visible and near-infrared excitation sources (Figure 5). The N-CNDs exhibited good cell permeability, minimal cytotoxicity at concentration levels below 0.5 mg mL^{-1} (Figure S6) and a remarkable fluorescent signal upon multi-photon excitation at 740 nm thereby corroborating the up-converting response of the N-CNDs and opening an important synthetic alternative to expensive and less stable NIR dyes and the potential capability to monitor multiple cell processes and induce therapeutic treatments with minimal tissue damages and maximum penetration depth.

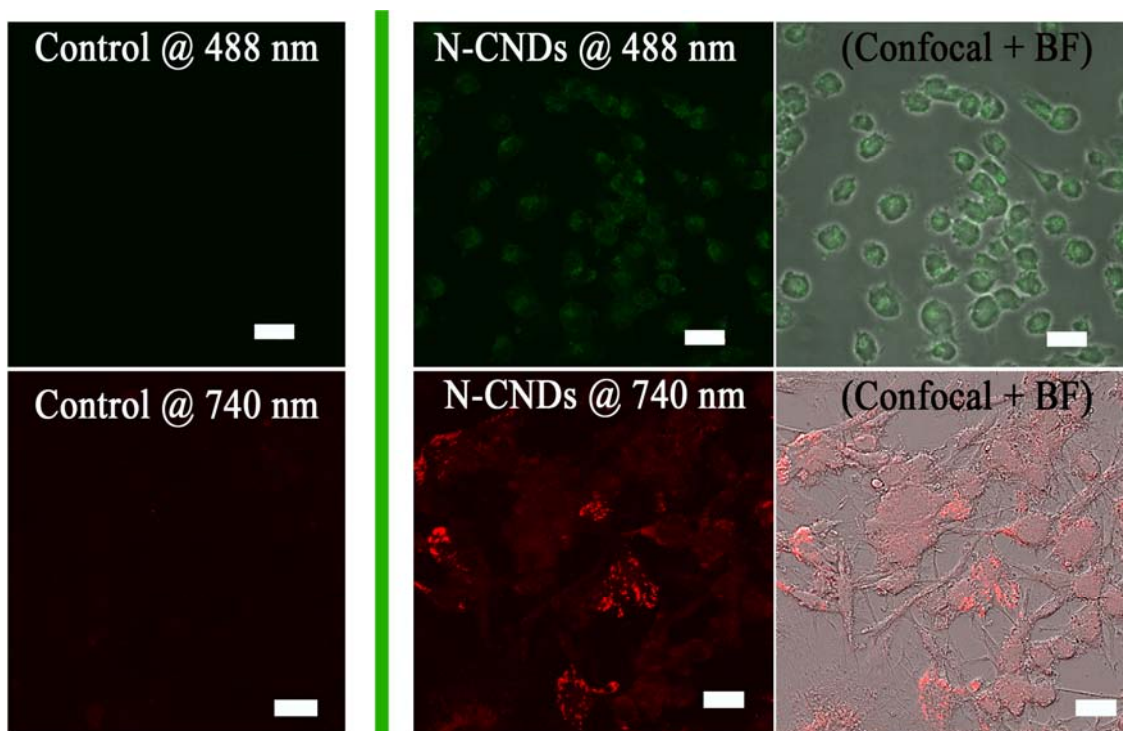


Figure 5. Confocal fluorescence microphotographs of U251MG glioma cells after 24 hours of incubation at 37 °C using $\lambda_{exc} = 488$ nm (top-panel images) and $\lambda_{exc} = 740$ nm (down-panel images), respectively; The control images correspond to unlabeled cells. The N-CNDs were co-incubated at 0.02 and 0.2 mg mL⁻¹ concentrations for the down and upconversion induced imaging in the visible and NIR ranges, respectively. The images on the right correspond to the overlay of confocal and bright field microphotographs. The detection wavelength range was 400-600 nm. All the scale bars correspond to 20 μ m.

4. Conclusions

In this study, we have shown a simple and cost-effective hydrothermal assisted method to induce the transformation of vitamin C (ascorbic acid) into multifunctional carbon nanodots with different and appealing optical properties such as expanded photoluminescence in the visible-NIR range (down and up-conversion behavior) for cell bioimaging, pH dependent lifetime decay response or enhanced selectivity towards the detection of copper ions, even in the presence of highly interfering ion counterparts such as iron that can be selectively minimized in the NIR detection range. Furthermore, the crucial influence of ethanolamine in the N-doping process of the carbon dots to enhance these properties is clearly demonstrated.

Acknowledgements

People Program (CIG-Marie Curie Actions, REA grant agreement n° 294094, NANOLIGHT) is gratefully acknowledged.

References

- [1] M.J. Ruedas-Rama, A. Orte, E.A.H. Hall, J.M. Alvarez-Pez, E.M. Talavera, Quantum dot photoluminescence lifetime-based pH nanosensor, *Chem. Commun.* 47 (2011) 2898-2900.
- [2] J. Zhang, B. Li, L.M. Zhang, H. Jiang, An optical sensor for Cu(II) detection with upconverting luminescent nanoparticles as an excitation source, *Chem. Commun.* 48 (2012) 4860-4862.
- [3] A. Salinas-Castillo, M. Ariza-Avidad, C. Pritz, M. Camprubi-Robles, B. Fernandez, M.J. Ruedas-Rama, A. Megia-Fernandez, A. Lapresta-Fernandez, F. Santoyo-Gonzalez, A. Schrott-Fischer, L.F. Capitan-Vallvey, Carbon dots for copper detection with down and upconversion fluorescent properties as excitation sources, *Chem. Commun.* 49 (2013) 1103-1105.
- [4] J.H. Shen, Y.H. Zhu, X.L. Yang, C.Z. Li, Graphene quantum dots: emergent nanolights for bioimaging, sensors, catalysis and photovoltaic devices, *Chem. Commun.* 48 (2012) 3686-3699.
- [5] S.J. Zhu, Y.B. Song, X.H. Zhao, J.R. Shao, J.H. Zhang, B. Yang, The photoluminescence mechanism in carbon dots (graphene quantum dots, carbon nanodots, and polymer dots): current state and future perspective, *Nano Res.* 8 (2015) 355-381.

- [6] P. Roy, P.C. Chen, A.P. Periasamy, Y.N. Chen, H.T. Chang, Photoluminescent carbon nanodots: synthesis, physicochemical properties and analytical applications, *Mater. Today* 18 (2015) 447-458.
- [7] S.N. Baker, G.A. Baker, Luminescent Carbon Nanodots: Emergent Nanolights, *Angew. Chem.-Int. Edit.* 49 (2010) 6726-6744.
- [8] C.T. Chien, S.S. Li, W.J. Lai, Y.C. Yeh, H.A. Chen, I.S. Chen, L.C. Chen, K.H. Chen, T. Nemoto, S. Isoda, M.W. Chen, T. Fujita, G. Eda, H. Yamaguchi, M. Chhowalla, C.W. Chen, Tunable Photoluminescence from Graphene Oxide, *Angew. Chem.-Int. Edit.* 51 (2012) 6662-6666.
- [9] Y.Q. Dong, H.C. Pang, H.B. Yang, C.X. Guo, J.W. Shao, Y.W. Chi, C.M. Li, T. Yu, Carbon-Based Dots Co-doped with Nitrogen and Sulfur for High Quantum Yield and Excitation-Independent Emission, *Angew. Chem.-Int. Edit.* 52 (2013) 7800-7804.
- [10] H.P. Liu, T. Ye, C.D. Mao, Fluorescent carbon nanoparticles derived from candle soot, *Angew. Chem.-Int. Edit.* 46 (2007) 6473-6475.
- [11] K. Lingam, R. Podila, H.J. Qian, S. Serkiz, A.M. Rao, Evidence for Edge-State Photoluminescence in Graphene Quantum Dots, *Adv. Funct. Mater.* 23 (2013) 5062-5065.
- [12] S. Liu, J.Q. Tian, L. Wang, Y.W. Zhang, X.Y. Qin, Y.L. Luo, A.M. Asiri, A.O. Al-Youbi, X.P. Sun, Hydrothermal Treatment of Grass: A Low-Cost, Green Route to Nitrogen-Doped, Carbon-Rich, Photoluminescent Polymer Nanodots as an Effective Fluorescent Sensing Platform for Label-Free Detection of Cu(II) Ions, *Adv. Mater.* 24 (2012) 2037-2041.
- [13] H. Tetsuka, R. Asahi, A. Nagoya, K. Okamoto, I. Tajima, R. Ohta, A. Okamoto, Optically Tunable Amino-Functionalized Graphene Quantum Dots, *Adv. Mater.* 24 (2012) 5333-5338.

- [14] X. Guo, C.F. Wang, Z.Y. Yu, L. Chen, S. Chen, Facile access to versatile fluorescent carbon dots toward light-emitting diodes, *Chem. Commun.* 48 (2012) 2692-2694.
- [15] S. Karthik, B. Saha, S.K. Ghosh, N.D.P. Singh, Photoresponsive quinoline tethered fluorescent carbon dots for regulated anticancer drug delivery, *Chem. Commun.* 49 (2013) 10471-10473.
- [16] C.H. Lee, R. Rajendran, M.S. Jeong, H.Y. Ko, J.Y. Joo, S. Cho, Y.W. Chang, S. Kim, Bioimaging of targeting cancers using aptamer-conjugated carbon nanodots, *Chem. Commun.* 49 (2013) 6543-6545.
- [17] D.Y. Pan, J.C. Zhang, Z. Li, C. Wu, X.M. Yan, M.H. Wu, Observation of pH-, solvent-, spin-, and excitation-dependent blue photoluminescence from carbon nanoparticles, *Chem. Commun.* 46 (2010) 3681-3683.
- [18] Q. Qu, A.W. Zhu, X.L. Shao, G.Y. Shi, Y. Tian, Development of a carbon quantum dots-based fluorescent Cu²⁺ probe suitable for living cell imaging, *Chem. Commun.* 48 (2012) 5473-5475.
- [19] J.H. Shen, Y.H. Zhu, C. Chen, X.L. Yang, C.Z. Li, Facile preparation and upconversion luminescence of graphene quantum dots, *Chem. Commun.* 47 (2011) 2580-2582.
- [20] W.B. Shi, Q.L. Wang, Y.J. Long, Z.L. Cheng, S.H. Chen, H.Z. Zheng, Y.M. Huang, Carbon nanodots as peroxidase mimetics and their applications to glucose detection, *Chem. Commun.* 47 (2011) 6695-6697.
- [21] Y.P. Sun, B. Zhou, Y. Lin, W. Wang, K.A.S. Fernando, P. Pathak, M.J. Mezziani, B.A. Harruff, X. Wang, H.F. Wang, P.J.G. Luo, H. Yang, M.E. Kose, B.L. Chen, L.M. Veca, S.Y. Xie, Quantum-sized carbon dots for bright and colorful photoluminescence, *J. Am. Chem. Soc.* 128 (2006) 7756-7757.

- [22] S.T. Yang, L. Cao, P.G.J. Luo, F.S. Lu, X. Wang, H.F. Wang, M.J. Meziari, Y.F. Liu, G. Qi, Y.P. Sun, Carbon Dots for Optical Imaging in Vivo, *J. Am. Chem. Soc.* 131 (2009) 11308-+.
- [23] S.J. Zhu, S.J. Tang, J.H. Zhang, B. Yang, Control the size and surface chemistry of graphene for the rising fluorescent materials, *Chem. Commun.* 48 (2012) 4527-4539.
- [24] H. Nie, M.J. Li, Q.S. Li, S.J. Liang, Y.Y. Tan, L. Sheng, W. Shi, S.X.A. Zhang, Carbon Dots with Continuously Tunable Full-Color Emission and Their Application in Ratiometric pH Sensing, *Chem. Mat.* 26 (2014) 3104-3112.
- [25] M.C. Ortega-Liebana, J.L. Hueso, A. Larrea, V. Sebastian, J. Santamaria, Feroxyhyte nanoflakes coupled to up-converting carbon nanodots: a highly active, magnetically recoverable, Fenton-like photocatalyst in the visible-NIR range, *Chem. Commun.* 51 (2015) 16625-16628.
- [26] F. Wang, Z. Xie, H. Zhang, C.Y. Liu, Y.G. Zhang, Highly Luminescent Organosilane-Functionalized Carbon Dots, *Adv. Funct. Mater.* 21 (2011) 1027-1031.
- [27] L.W. Zhang, H.B. Fu, Y.F. Zhu, Efficient TiO₂ photocatalysts from surface hybridization of TiO₂ particles with graphite-like carbon, *Adv. Funct. Mater.* 18 (2008) 2180-2189.
- [28] B. Kong, A.W. Zhu, C.Q. Ding, X.M. Zhao, B. Li, Y. Tian, Carbon Dot-Based Inorganic-Organic Nanosystem for Two-Photon Imaging and Biosensing of pH Variation in Living Cells and Tissues, *Adv. Mater.* 24 (2012) 5844-5848.
- [29] M.C. Ortega-Liebana, J.L. Hueso, S. Ferdousi, K.L. Yeung, J. Santamaria, Nitrogen-doped luminescent carbon nanodots for optimal photo-generation of hydroxyl radicals and visible-light expanded photo-catalysis, *Diam. Relat. Mater.* 65 (2016) 176-182.

- [30] H.T. Li, Z.H. Kang, Y. Liu, S.T. Lee, Carbon nanodots: synthesis, properties and applications, *J. Mater. Chem.* 22 (2012) 24230-24253.
- [31] P.J.G. Luo, S. Sahu, S.T. Yang, S.K. Sonkar, J.P. Wang, H.F. Wang, G.E. LeCroy, L. Cao, Y.P. Sun, Carbon "quantum" dots for optical bioimaging, *J. Mat. Chem. B* 1 (2013) 2116-2127.
- [32] Z.F. Wang, H.D. Zeng, L.Y. Sun, Graphene quantum dots: versatile photoluminescence for energy, biomedical, and environmental applications, *J. Mater. Chem. C* 3 (2015) 1157-1165.
- [33] Y.B. Song, S.J. Zhu, B. Yang, Bioimaging based on fluorescent carbon dots, *RSC Adv.* 4 (2014) 27184-27200.
- [34] W.P. Wang, Y.C. Lu, H. Huang, A.J. Wang, J.R. Chen, J.J. Feng, Facile synthesis of N, S-codoped fluorescent carbon nanodots for fluorescent resonance energy transfer recognition of methotrexate with high sensitivity and selectivity, *Biosens. Bioelectron.* 64 (2015) 517-522.
- [35] H.T. Li, X.D. He, Y. Liu, H. Huang, S.Y. Lian, S.T. Lee, Z.H. Kang, One-step ultrasonic synthesis of water-soluble carbon nanoparticles with excellent photoluminescent properties, *Carbon* 49 (2011) 605-609.
- [36] H.Q. Tao, K. Yang, Z. Ma, J.M. Wan, Y.J. Zhang, Z.H. Kang, Z. Liu, In Vivo NIR Fluorescence Imaging, Biodistribution, and Toxicology of Photoluminescent Carbon Dots Produced from Carbon Nanotubes and Graphite, *Small* 8 (2012) 281-290.
- [37] A.M. Brouwer, Standards for photoluminescence quantum yield measurements in solution (IUPAC Technical Report), *Pure Appl. Chem.* 83 (2011) 2213-2228.
- [38] J.R. Lakowicz, *Principles of Fluorescence Spectroscopy*, Third Edition ed., Springer US, 2006.

- [39] M. Algarra, B.B. Campos, K. Radotic, D. Mutavdzic, T. Bandosz, J. Jimenez-Jimenez, E. Rodriguez-Castellon, J. da Silva, Luminescent carbon nanoparticles: effects of chemical functionalization, and evaluation of Ag⁺ sensing properties, *J. Mater. Chem. A* 2 (2014) 8342-8351.
- [40] J.L. Hueso, J.P. Espinos, A. Caballero, J. Cotrino, A.R. Gonzalez-Elipe, XPS investigation of the reaction of carbon with NO, O-2, N-2 and H2O plasmas, *Carbon* 45 (2007) 89-96.
- [41] A. Eguizabal, L. Uson, V. Sebastian, J.L. Hueso, M.P. Pina, Efficient and facile tuning of Vulcan XC72 with ultra-small Pt nanoparticles for electrocatalytic applications, *RSC Adv.* 5 (2015) 90691-90697.
- [42] X.Y. Zhai, P. Zhang, C.J. Liu, T. Bai, W.C. Li, L.M. Dai, W.G. Liu, Highly luminescent carbon nanodots by microwave-assisted pyrolysis, *Chem. Commun.* 48 (2012) 7955-7957.
- [43] A. Orte, J.M. Alvarez-Pez, M.J. Ruedas-Rama, Fluorescence Lifetime Imaging Microscopy for the Detection of Intracellular pH with Quantum Dot Nanosensors, *ACS Nano* 7 (2013) 6387-6395.
- [44] Y.Q. Dong, R.X. Wang, G.L. Li, C.Q. Chen, Y.W. Chi, G.N. Chen, Polyamine-Functionalized Carbon Quantum Dots as Fluorescent Probes for Selective and Sensitive Detection of Copper Ions, *Anal. Chem.* 84 (2012) 6220-6224.
- [45] J. Zong, X.L. Yang, A. Trinchi, S. Hardin, I. Cole, Y.H. Zhu, C.Z. Li, T. Muster, G. Wei, Carbon dots as fluorescent probes for "off-on" detection of Cu²⁺ and L-cysteine in aqueous solution, *Biosens. Bioelectron.* 51 (2014) 330-335.
- [46] M. Vedamalai, A.P. Periasamy, C.W. Wang, Y.T. Tseng, L.C. Ho, C.C. Shih, H.T. Chang, Carbon nanodots prepared from o-phenylenediamine for sensing of Cu²⁺ ions in cells, *Nanoscale* 6 (2014) 13119-13125.